JOURNAL OF CHEMICAL & ENGINEERING DATA

ARTICLE

pubs.acs.org/jced

Screening Zeolites for Gas Separation Applications Involving Methane, Nitrogen, and Carbon Dioxide

Nathan K. Jensen,[†] Thomas E. Rufford,[†] Guillaume Watson,[†] Dongke K. Zhang,[†] K. Ida Chan,[‡] and Eric F. May*[,†]

[†]Centre for Energy, The University of Western Australia, 35 Stirling Highway, Crawley WA 6009, Australia

[‡]Chevron Energy Technology Company, Houston, Texas 77002, United States

Supporting Information

ABSTRACT: An experimental evaluation of the kinetics and equilibrium capacities of pure fluids as a fast and effective means to screen an adsorbent's gas separation potential is described. Equilibrium adsorption capacities for pure N_2, CH_4, and CO_2 have been determined using a Micromeritics ASAP2020 sorption analyzer, for three commercially available zeolites: natural chabazite, H^+ mordenite, and Linde 4A molecular sieve over the temperature range from (248 to 302) K and pressure range from (0.001 to 120) kPa. Toth models were regressed to the equilibrium data for each gas and used to generate inferred equilibrium selectivity maps over a wider range of temperature and pressure for the purpose of targeting any future mixture measurements. For each gas, the rate of adsorption at 100 kPa was measured as a function of temperature and used with a linear driving force model to calculate mass transfer coefficients. In most cases the ratio of the mass transfer coefficients for each pair of gases was close to unity and did not give rise to a significant kinetic selectivity. However the Linde 4A molecular sieve at 273 K and 100 kPa had a kinetic selectivity for CO_2 over CH_4 of 6.2. This approach to screening adsorbents with pure fluids can assist in optimizing the design of subsequent mixture measurements by identifying the most promising temperature and pressure ranges to target.

INTRODUCTION

In 2010, 23.8 % of global energy consumption was supplied by natural gas, and if the current trends continue along with increasing regulation and financial penalties imposed on carbon emissions, the volume of natural gas consumed is predicted to grow by 50 %[1] over the next 20 years. Natural gas consists predominantly of methane (80 % to 95 %), with varying amounts of heavier hydrocarbons, sulfur-containing compounds, CO_2, and inert gases such as N_2 (with trace concentrations of helium) depending on the location and age of the reserve. Many significant natural gas reserves contain high levels of CO_2 and N_2; for example, many proven reserves contain sub-quality gas with concentrations greater than 4 % N_2 and 4 % CO_2,[2] and to meet gas pipeline specifications the N_2 and CO_2 concentrations must be reduced to typically less than 3 % N_2 and less than 2 % CO_2.[3] The volume of natural gas traded as liquefied natural gas (LNG) has increased in recent years (31 % of the gas traded in 2010 was as LNG[4]), and because, for example, CO_2 can freeze in the cryogenic liquefaction, the specifications on the quality of natural gas feed to a LNG plant are stricter than for pipeline gas. The maximum CO_2 concentration in LNG feed gas should not be more than 50 ppmv. High N_2 concentrations in the LNG feed gas can reduce significantly the efficiency of the liquefaction process because the additional N_2 must be cooled along with the CH_4 to the liquefaction temperature (approximately 111 K).

The most common technology used to remove CO_2 from natural gas is amine scrubbing in gas−liquid contactors. Conventional aqueous amine absorption processes are energy-intensive because high temperatures are required to regenerate the saturated amine solvent, involving highly corrosive solvents, and the cost of the process scales almost linearly with the volume of CO_2 to be removed. Nitrogen is normally rejected from natural gas by cryogenic distillation. Cryogenic N_2 rejection units require large amounts of energy to achieve the temperatures needed for separation of CH_4 and N_2, and these units are typically only economically viable for natural gas plants processing more than 15 MMscfd gas.[5] Pressure swing adsorption (PSA) has been proposed as a possible alternative technology for both CO_2 and N_2 separation from natural gas[6−8] because adsorption-based processes have lower energy requirements and lower capital investment costs than amine scrubbers or cryogenic distillation units. However, a key challenge in developing efficient PSA processes for the separation of CO_2 and N_2 from natural gas is identifying suitable adsorbents with high selectivity and adsorption capacity.

A number of adsorbent materials have been proposed and tested for PSA separation, ranging from carbon molecular sieves[9−12] and zeolites[6,13−16] to inorganic and organic metal complexes.[17−19] While Engelhard's patented ETS-4[16,20,21] and its derivatives are the current benchmarks for N_2 and CH_4 separation, there are many adsorbent materials with comparable pore sizes to ETS-4 that may deliver similar or improved separation performance, particularly given the wider range of temperatures and pressures accessible in an LNG plant. Similarly, while commercial adsorption processes exist for removing CO_2 to meet the requisite LNG specification (for example, UOP's MOLSIV process using the adsorbent 4A-LNG[22]), it may be

Received: July 29, 2011
Accepted: October 4, 2011
Published: October 27, 2011

possible to further optimize such processes by operating them with different adsorbents or at different temperature and pressure conditions. Most data sets available in the literature even for well-characterized adsorbents are limited in that they were measured at near or above ambient temperatures. Furthermore, many novel adsorbent materials are continuously being developed for a variety of applications that may provide superior separation performance for many different gases. To screen the large number of potential adsorbents and range of conditions as part of the search for an improved separation process, it is essential that the set of experiments undertaken provide the necessary information as efficiently as possible.

Any such screening method must start with an evaluation of the adsorbent's pure fluid kinetics and equilibrium capacities. In this work three commercially available zeolite materials, natural chabazite, H^+ mordenite, and Linde 4A molecular sieve, were screened to determine their equilibrium and kinetic sorption parameters for CH_4, N_2, and CO_2, with a view to their potential for treating contaminated natural gas destined for conversion to LNG. The purpose of this paper is to report the results of those measurements and describe the method and analysis used to assess whether future mixture measurements should be conducted and, if so, at which conditions they should be targeted.

MATERIALS

The natural chabazite was provided by Zeox Corporation (Tucson, AZ, USA), the synthetic H+ mordenite by TOSOH Corporation (Tokyo, Japan), and the synthetic Linde 4A zeolite by Sigma-Aldrich (Castle Hill, NSW, Australia). The chabazite source was a natural deposit located in Bowie, Arizona. The chabazite sample was in the form of granules with a size between (1 and 5) mm. The mordenite and Linde 4A samples were 3 mm extruded pellets. All gases used for analysis were ultrahigh purity supplied by BOC Australia, with the following specified purities: 99.999 % CH_4, 99.999 % N_2, and 99.99% CO_2.

Powder X-ray diffraction (Siemens D5000 powder XRD) was used to determine the phase structure and to identify any impurities in the chabazite sample; the XRD patterns are provided in the Supporting Information (SI) of this paper and show small impurities most likely to be naturally occurring silica-based products. The silica-to-alumina ratio of the chabazite was determined by X-ray fluorescence spectroscopy to be 3.7 (Philips 2404 XRF). The principal cations identified by XRF in the chabazite were Na^+ and Mg^{2+}. According to the manufacturers' data, the silica-to-alumina ratios of Linde 4A and H^+ mordenite were 1.1 and 18, respectively. The pore textural properties of each adsorbent were characterized by sorption analyses with N_2 at 77 K and CO_2 at 273 K using the Micromeritics ASAP2020[23] instrument. Prior to each adsorption measurement, 1 g of the selected adsorbent was degassed under vacuum at 623 K for 12 h.

MEASUREMENTS AND ANALYSIS

Equilibrium and kinetic adsorption measurements were measured volumetrically with the Micromeritics ASAP2020 at three temperatures (248, 273, and 302) K and over the pressure range (0.05 to 120) kPa for CH_4 and N_2 and (0.001 to 120) kPa for CO_2. The kinetic measurements were taken concurrently with the equilibrium measurements, following a similar method to that described by Saha et al.[18] The adsorbate gas was introduced into the sample cell at a given pressure, and the change in gas pressure was recorded as a function of time. This recorded pressure change was converted to an adsorbed gas volume as a function of time. Once the sample cell pressure had stabilized after each kinetic measurement (criteria for equilibrium that the pressure change is less that 0.01 % in a selected time interval of 30 s), the final pressure was recorded and converted to an equilibrium adsorption capacity. The reversibility of the adsorption process for each adsorbate−adsorbent pair was checked by also measuring desorption isotherms.

Equilibrium data for each adsorbate−absorbent combination were regressed using a temperature-dependent Toth model[24] as follows

$$Q_i = Q_{mi}\frac{K_iP}{[1 + (K_iP)^{n_i}]^{1/n_i}} \tag{1a}$$

$$K_i = K_i^{o}\exp\left(-\frac{\Delta H_i}{RT}\right) \tag{1b}$$

Here, Q_i and Q_{mi} are the amounts of gas i adsorbed a given pressure and at infinite pressure, respectively, ΔH_i is the isosteric enthalpy of adsorption at zero loading, n_i is a parameter describing surface heterogeneity, R is the gas constant, T is the measurement temperature, and K_i^{o} is the adsorption Henry constant at infinite temperature. The Toth model offers several advantages for predicting adsorption on microporous solids: using only four parameters (n_i, ΔH_i, Q_{mi}, and K_i^{o}), the Toth equation provides an analytical expression for Q_i that is an explicit function of temperature and pressure. Furthermore, at low partial pressures the Toth equation reduces to Henry's law, and when the parameter $n_i = 1$ it reduces to the Langmuir function.

The linear driving force (LDF) model[25] was used to estimate a mass transfer coefficient, κ_i, for each adsorbate−adsorbent combination from the time-dependent adsorption data. According to this model, the relationship between the time-dependent fractional uptake, $F_i(t) \equiv (Q_i(t) - Q_i(0))/(Q_i(\infty) - Q_i(0))$, and the mass transfer coefficient is

$$1 - F_i = \exp(-\kappa_i t) \tag{2}$$

The value of the mass transfer coefficient can be determined using a least-squares regression of eq 2 to the time-dependent F_i data (as shown in Figure 6A). However, in some cases the noise and limited resolution of the time-dependent data (shown in Figure 6B) collected meant that more reliable values of κ_i could be obtained by linear regression of $\ln(1 - F_i)$ as a function of time at a given pressure, with the slope of the fitted line being equal to $-\kappa_i$. The mass transfer coefficient can be interpreted in terms of a diffusive time constant $(D_{c,i}/r_c^2)^{-1}$, as described for example by Saha et al.[18] where $D_{c,i}$ and r_c are the intracrystalline diffusivity and equivalent crystal radius, respectively. However, as discussed by Sircar and Hufton,[25] such an identification can be (i) erroneous if the uptake experiment does not strictly conform with the assumptions inherent to the Fickian-diffusion analysis, and (ii) unnecessary for the purposes of practical process design.

An adsorbent's equilibrium selectivity, α_{ij}, for two components in a gas mixture (i is the more adsorbed component and j the less adsorbed component) is defined (for example, Saha et al.[18]):

$$\alpha_{ij} \equiv \left(\frac{x_i}{x_j}\right)\left(\frac{y_j}{y_i}\right) \underset{y_j = y_i}{\rightarrow} \alpha_{ij} = \left(\frac{Q_i}{Q_j}\right) \tag{3}$$

Here, y and x are the mole fractions of a component in the vapor and adsorbed phase, respectively, and the second equality holds in

dx.doi.org/10.1021/je200817w |J. Chem. Eng. Data 2012, 57, 106–113

the case of an equimolar mixture. Clearly the design of any gas separation process using an adsorbent will require measurements with mixtures; however, when screening a large number of adsorbents for a given gas separation application, it is useful to infer an equilibrium selectivity based on the results of pure fluid measurements (also sometimes referred to as an ideal selectivity[26]). In that case, the second equality in eq 3 can be used with values of Q_i and Q_j measured at identical conditions or calculated using a model such as eq 1 with appropriate parameters for each component listed.

Separations based on differences in sorption rates may still be possible even if $\alpha_{ij} \approx 1$. To quantify this it is convenient to define a kinetic selectivity factor, β_{ij}, which incorporates the effects of each component's sorption mass transfer coefficient.

$$\beta_{ij} \equiv \alpha_{ij}\sqrt{\frac{\kappa_i}{\kappa_j}}_{y_j=y_i} \rightarrow \beta_{ij} = \left(\frac{Q_i}{Q_j}\right)\sqrt{\frac{\kappa_i}{\kappa_j}} \quad (4)$$

As discussed recently by Ruthven,[27] the kinetic selectivity depends on both the diffusivity ratio (assuming $\kappa_i \propto D_{c,i}$) and the equilibrium selectivity, which if being inferred from pure fluid measurements can be estimated from the second equality in eq 4. Evaluating β_{ij} is thus an important part of screening potential adsorbents for a given gas separation application.

RESULTS AND DISCUSSION

Isotherms for the sorption of N_2 at 77 K on chabazite, H^+ mordenite, and Linde 4A are shown in Figure 1. For relative pressures below 0.1, mordenite and chabazite adsorbed significant volumes of N_2 and exhibited a type I isotherm according to the International Union of Pure and Applied Chemistry (IUPAC) specification, which indicates that these adsorbents contain a high volume-fraction of micropores.[28] The shape of the N_2 isotherms at relative pressures above 0.7 indicates the presence also of mesoporous and macroporous voids in the chabazite and mordenite.

A summary of the pore textural properties of the adsorbents is provided in Table 1. The specific surface areas calculated using the Brunauer–Emmett–Teller (BET) method[23] are 415 $m^2 \cdot g^{-1}$ and 363 $m^2 \cdot g^{-1}$ for chabazite and mordenite, respectively. Both of these BET values are lower than the specific surface areas calculated using the Dubinin–Radushkevich (DR) method[23] at the same conditions (N_2 at 77 K). These differences could be attributed to the BET model not accounting for micropore filling, therefore underestimating the surface area. Micropore volumes were calculated from the 77 K N_2 adsorption isotherm using the Horvath–Kawazoe (HK) method;[23] the results are listed in Table 1.

The Linde 4A isotherm in Figure 1 shows that at 77 K only a small amount of N_2 is adsorbed at low relative pressures and the uptake of N_2 does not begin to increase significantly until a relative pressure of at least 0.8 when the N_2 starts to fill void spaces between the zeolite crystals. The uptake of N_2 on Linde 4A is low in this measurement because the diffusion of the N_2 molecule (kinetic diameter: 0.364 nm) into the narrow pores of zeolite 4A (pore aperture 0.39 nm) is kinetically hindered at 77 K.[29] Thus, the BET model is not applicable for determining the surface area of the Linde 4A zeolite with N_2 at 77 K. To overcome this limitation of the N_2 sorption analyses, CO_2 adsorption at 273 K was used as a complementary technique to determine the micropore surface area and micropore volume using the DR method, which are listed in Table 1. For the purpose of comparison between all three adsorbents, the DR surface area and micropore volume of the chabazite and mordenite calculated using CO_2 adsorption isotherms measured at 273 K are also listed.

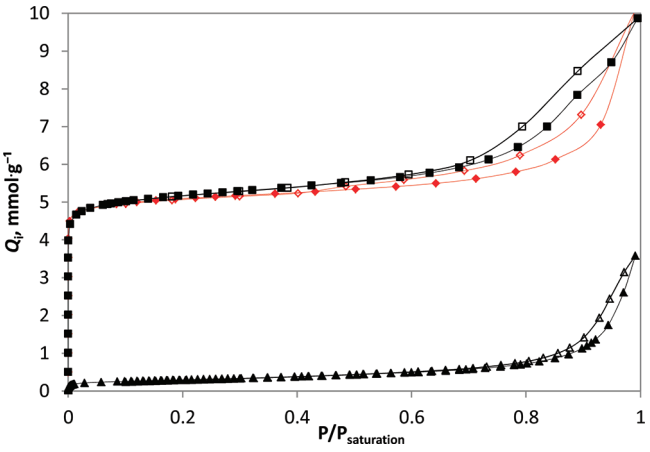

Figure 1. Nitrogen adsorption (solid symbols)/desorption (open symbols) isotherms at 77 K on natural chabazite, red ◆; H^+ mordenite, ■; and Linde 4A, ▲.

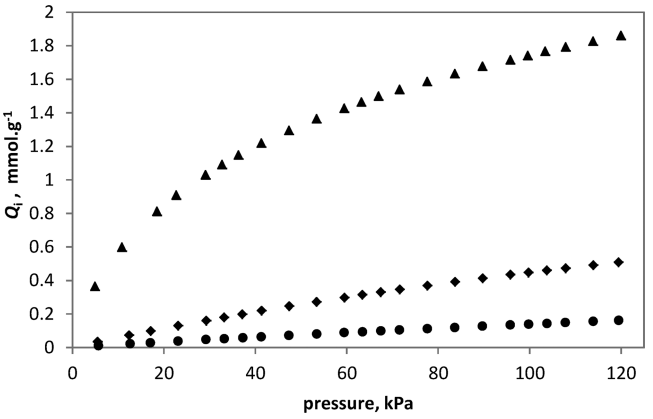

Figure 2. Measured equilibrium adsorption capacities at 303 K for H^+ mordenite with CH_4, ◆; N_2, ●; and CO_2, ▲.

Table 1. BET Specific Surface Area, DR Surface Area, HK Micropore Volume, and Total Pore Volume of the Adsorbents Derived from Sorption Experiments with N_2 at 77 K and DR Surface Area and DR Micropore Volume of the Adsorbents Derived from Sorption Experiments with CO_2 at 273 K

	BET surface area	total pore volume	HK micropore volume	N_2 DR surface area	CO_2 DR surface area	DR micropore volume
sample	$m^2 \cdot g^{-1}$	$cc \cdot g^{-1}$	$cc \cdot g^{-1}$	$m^2 \cdot g^{-1}$	$m^2 \cdot g^{-1}$	$cc \cdot g^{-1}$
chabazite	415	0.348	0.171	489	454	0.182
Linde 4A		0.108			402	0.161
H^+ mordenite	363	0.340	0.174	492	417	0.167

dx.doi.org/10.1021/je200817w |J. Chem. Eng. Data 2012, 57, 106–113

Table 2. Parameters of the Toth Model (Equation 1) Fitted to the Adsorption Capacities for Each Pure Gas Measured at Temperatures of (248, 273, and 302) K and Pressures to 120 kPa. For Linde 4A the Constraint n_{CH_4} = 1 Was Required

		Q_{mi}		$10^6\ K_i^\circ$		$-\Delta H_i$				rms deviation
adsorbent	gas	mmol·g^{-1}		kPa^{-1}		kJ·mol^{-1}		n_i		mmol·g^{-1}
chabazite	CH_4	2.04	± 0.01	1.31	± 0.05	22.67	± 0.08	0.80	± 0.01	0.01
	N_2	2.18	± 0.02	0.50	± 0.01	21.96	± 0.04	0.82	± 0.01	0.004
	CO_2	4.20	± 0.04	0.02	± 0.01	45.40	± 1.07	0.48	± 0.02	0.18
Linde 4A	CH_4	3.16	± 0.05	0.69	± 0.04	19.80	± 0.16	1.00		0.02
	N_2	8.6	± 3.4	0.003	± 0.001	28.22	± 0.33	0.51	± 0.08	0.02
	CO_2	4.37	± 0.07	0.50	± 0.02	38.30	± 0.48	0.38	± 0.02	0.20
H^+ mordenite	CH_4	2.16	± 0.09	0.33	± 0.02	22.76	± 0.09	0.91	± 0.03	0.004
	N_2	2.90	± 1.69	0.11	± 0.06	21.46	± 0.20	0.81	± 0.19	0.003
	CO_2	4.19	± 0.09	0.51	± 0.04	28.55	± 0.20	0.47	± 0.01	0.02

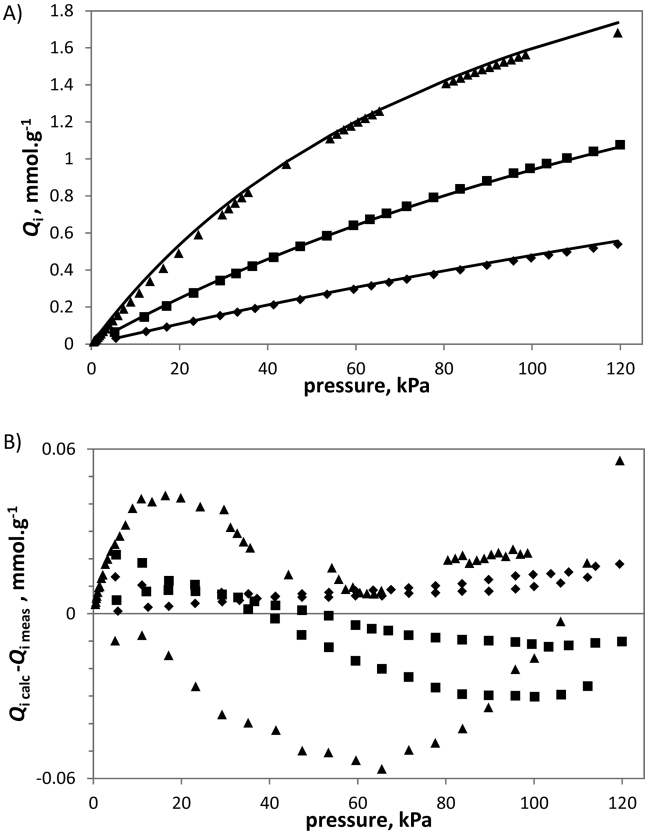

Figure 3. Adsorption of CH_4 on Linde 4A at 248 K, ●; 273 K, ▲; and 302 K, ◆. (A) Equilibrium capacities measured ($Q_{i,meas}$) and calculated ($Q_{i,calc}$) using the Toth model (eq 1) with the best-fit parameters listed in Table 2. (B) Deviations of the measured data from the best-fit model. For clarity, measured desorption data points are only shown in B.

Tabulated experimental results from the equilibrium adsorption measurements made in this work are included in the SI for this paper for readers who wish to make direct comparisons with our data and/or fit other adsorption models to the data. As an example of the relative uptakes of the different gases on a given adsorbent at a fixed temperature, Figure 2 shows the 302 K adsorption isotherms for N_2, CH_4, and CO_2 on H^+ mordenite. The equilibrium adsorption capacities under all measured conditions

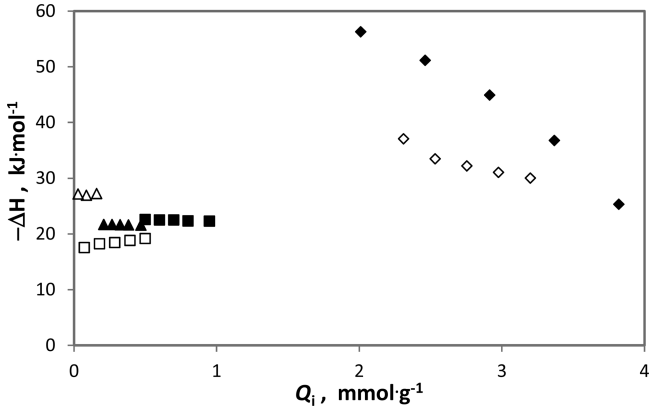

Figure 4. Isosteric enthalpies of adsorption for finite loadings on chabazite (solid symbols) and Linde 4A (open symbols) for CH_4, ■; N_2, ▲; and CO_2, ◆.

for all three adsorbents increased in order of N_2 < CH_4 < CO_2. For each gas the adsorption capacities increased with decreasing temperature. For each adsorbent most of the CO_2 uptake occurred at pressures below 5 kPa, with similar results at low pressure to those reported by Ridha et al.[30] These observations can be attributed to the strong electrostatic interactions between the quadrupole of the CO_2 molecule and the charge balancing cations within the zeolite structure.

The equilibrium adsorption capacities on H^+ mordenite at 100 kPa and 273 K were 0.33 mmol·g^{-1} for N_2, 0.92 mmol·g^{-1} for CH_4, and 2.49 mmol·g^{-1} for CO_2. These results are within 10 % of the adsorption capacities for each gas reported by Delgado et al.[31] at this condition. The adsorption capacities measured for Linde 4A at this condition are within 5% of the results published by Habgood.[32] Very little experimental data could be found for natural chabazite although Ridha et al.[30] measured the adsorption of N_2 and CO_2 on a synthetic chabazite decomposed from zeolite X. At 273 K and 100 kPa, the N_2 and CO_2 adsorption capacities observed in our measurements are approximately 10 % lower than the results with the synthetic chabazite reported by Ridha et al.[30]

The measured equilibrium adsorption data for each gas on each adsorbent were regressed to the Toth model shown in eq 1. The optimized parameters and their statistical uncertainties are listed in Table 2 together with the root-mean-square (rms) deviation of the data from the regressed model. As an example,

dx.doi.org/10.1021/je200817w |J. Chem. Eng. Data 2012, 57, 106–113

Figure 3 shows the results of the Toth fit to the measured CH_4 adsorption on chabazite at (302, 273, and 248) K. Since all of the adsorption experiments were reversible, the desorption isotherms are not shown in Figure 3(A) for clarity; however they are shown as part of the residuals ($Q_{i,calc} - Q_{i,meas}$) in Figure 3B to indicate the fit quality and the small magnitude of any hysteresis. No adsorption experiments were completed for H^+ mordenite at a temperature of 248 K because the adsorption capacities and selectivities for H^+ mordenite observed in measurements at the higher temperatures were clearly lower than for the chabazite and Linde 4A (except for CH_4 at pressures < 50 kPa). Further the isosteric enthalpies of adsorption determined from the (302 and 273) K measurements indicated the capacities of mordenite would not increase sufficiently at 248 K to warrant the extra adsorption measurements.

The isosteric enthalpies of adsorption at finite loadings of each gas were estimated from the chabazite and Linde 4A data using the Clausius−Clapeyron equation and are shown in Figure 4. The isosteric enthalpies of adsorption for N_2 and CH_4 shown in Figure 4 are of a similar magnitude to the ΔH_{N_2} and ΔH_{CH_4} listed in Table 2 because they correspond to a near-zero coverage, approximating the definition of this parameter in eq 1. The strong interaction between CO_2 and the adsorbent surfaces is exemplified by the significant decrease in the magnitude of ΔH_{CO_2} as adsorption loading increases. For N_2 and CH_4 the isosteric enthalpies of adsorption are about half the magnitude of those for CO_2 and remain reasonably constant as adsorption loading increases. The measurement of the enthalpies of adsorption is particularly important for screening applications because they allow the likely gains in capacity with decreasing temperature to be assessed. Based on the ΔH_i parameters in Table 2, to effect a doubling in capacity at constant pressure the change in inverse temperature for all three adsorbents would need to be between (0.0002 and 0.0003) K^{-1} for N_2 and CH_4 and between (0.00013 and 0.00020) K^{-1} for CO_2. At 300 K, this amounts to temperature changes of (18 to 26) K and (11 to 18) K, respectively. Furthermore, the enthalpy of adsorption allows the estimation of the temperature below which no further increase in equilibrium capacity is likely to be realized at constant pressure. For example, at 100 kPa the predicted CH_4 capacity of the chabazite at 180 K is within 1 % of the value of $Q_{m,CH_4} = 2.04$ mmol·g^{-1}. Thus, while this is still well above the lowest temperatures available in an LNG plant, there would be no advantage in designing a chabazite-based PSA cycle below this temperature, and as a corollary there is no need to conduct mixture adsorption measurements at these low temperatures to improve the design basis for such a process. Of course, such a temperature represents a very significant extrapolation of the model beyond the range of the regressed data; it is quite possible that this capacity would not be achieved at that low temperature, for example because of changes in aperture size or diffusion rates at lower temperatures resulting in molecular sieving of the molecule as outlined by Breck.[29,33]

A key objective when screening adsorbents for a gas separation application is the development of predictive tools that can indicate likely pressure and temperature at which a PSA cycle may be most efficient. Given the time, cost, and difficulty of experimental adsorption measurements (especially at conditions far from ambient) and the large possible number of adsorbents that could be screened, the measurement program needs to be as efficient as possible: inaccurate predictive tools resulting from too few measurements are to be avoided, yet too many measurements will increase the cost in time and resources of the adsorbent screening to an unviable level. The two most important adsorption parameters in PSA cycle design are capacity and selectivity, and while mixture measurements will ultimately be required, the set of pure fluid measurements presented here are sufficient to estimate capacities and selectivities over a reasonably wide range of pressures and temperatures and thereby facilitate more targeted mixture measurements. The regression of the measured data for each fluid and adsorbent to the Toth model in eq 1 allows equilibrium capacities to be calculated with reasonable confidence over a wider range of conditions than the measurements themselves. Furthermore, these Toth models can be used to develop inferred equilibrium selectivity maps such as those shown in Figure 5.

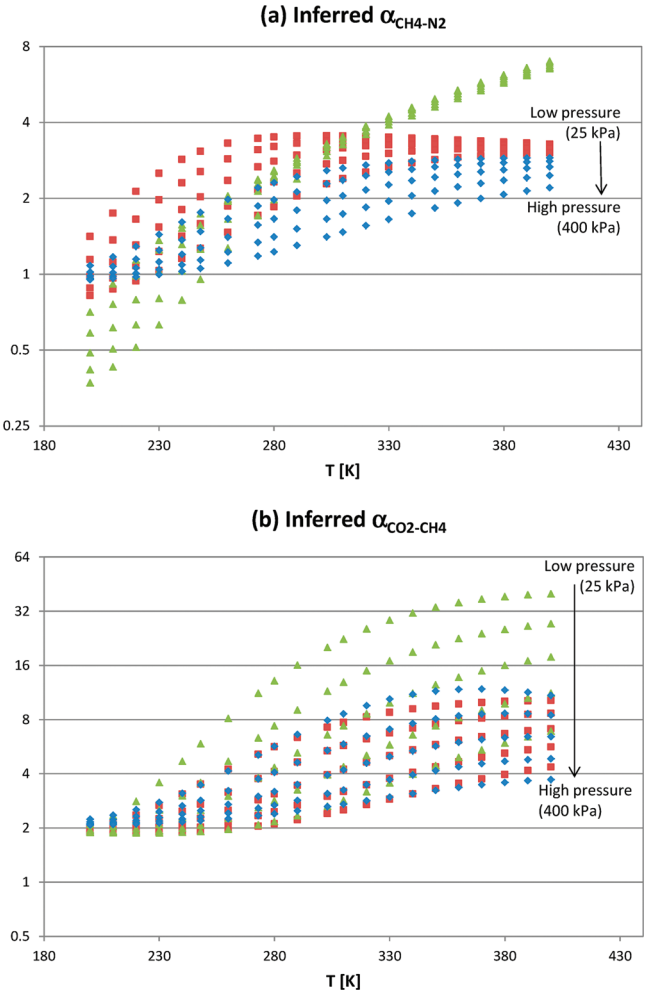

Figure 5. Inferred maps of equilibrium selectivities over the pressure range (25 to 400) kPa and temperature range (200 to 400) K, based on the four-parameter Toth models regressed to adsorption data measured in this work. (a) Inferred equilibrium selectivity for CH_4 over N_2, and (b) inferred equilibrium selectivity for CO_2 over CH_4, for chabazite, blue ◆; mordenite, red ■; and Linde 4A, green ▲.

Figure 5 shows the inferred $\alpha_{CH_4\text{-}N_2}$ and $\alpha_{CO_2\text{-}CH_4}$ values for chabazite, Linde 4A, and mordenite over the temperature range from (200 to 400) K and pressures from (25 to 400) kPa, calculated using eqs 1 and 3 and the appropriate parameters listed in Table 2. It should be noted that the arrows in Figure 5 indicate

dx.doi.org/10.1021/je200817w |J. Chem. Eng. Data 2012, 57, 106–113

Table 3. Mass Transfer Coefficients, κ_i, Inferred Equilibrium Selectivities, α_{ij}, and Inferred Kinetic Selectivities, β_{ij}, Derived from Adsorption Measurements at 100 kPa[a]

		$10^2\ \kappa_i\ (s^{-1})$			inferred equilibrium selectivity		inferred kinetic selectivity	
adsorbent	T/K	CH_4	N_2	CO_2	$\alpha_{CH_4\text{-}N_2}$	$\alpha_{CO_2\text{-}CH_4}$	$\beta_{CH_4\text{-}N_2}$	$\beta_{CO_2\text{-}CH_4}$
chabazite	302	2.7	3.0	1.2	1.9	3.9	1.8	2.6
	273	2.3	2.6	1.0	1.5	3.0	1.4	2.0
	248	3.0	2.1	1.4	1.3	2.6	1.5	1.8
Linde 4A	302	1.3	1.5	1.2	3.4	6.5	3.2	6.2
	273	0.6	1.5	1.7	2.4	3.7	1.5	6.2
	248	0.7	1.8	0.7	1.5	2.7	1.0	2.7
H^+ mordenite	302			2.0	3.2	3.8		
	273	3.5		1.8	2.8	2.8		2.0

[a] The relative uncertainties of κ_i, α_{ij}, and β_{ij} are estimated to be 50 %, 10 %, and 40 %, respectively. The time-dependent adsorption data measured for mordenite with N_2 and with CH_4 at 302 K were too noisy to allow satisfactory estimation of the corresponding κ_i values.

only the general direction of increasing pressure. The temperature and pressure bounds of the maps were chosen to illustrate both the scale of possible variation and the limiting behavior of $\alpha_{ij}(T,p)$ under the constraint of an equimolar vapor phase (second equality in eq 3). These inferred selectivity maps contain a moderate amount of extrapolation up in pressure and in both directions of temperature, and accordingly care should be taken when considering the predicted values. However, it is worth noting that the values of $\alpha_{CH_4\text{-}N_2}$ and $\alpha_{CO_2\text{-}CH_4}$ furthest from unity occur most often at pressures below 100 kPa. Further, the nature of the exponential function in eq 1b means that the α_{ij} are less sensitive to high temperature extrapolation. Thus, the inferred selectivity maps in Figure 5 are reasonable tools for conducting an initial assessment of an absorbent's potential gas separation applications and for identifying the most suitable temperatures and pressures to conduct subsequent mixture measurements.

As shown in Figure 5a, $\alpha_{CH_4\text{-}N_2}$ for Linde 4A has the strongest temperature dependence, ranging from 0.37 (N_2 selective) at (200 K, 400 kPa) to 6.5 (CH_4 selective) at (400 K, 25 kPa). In contrast, chabazite and mordenite have $\alpha_{CH_4\text{-}N_2} \geq 1$ within this range and with less variation. Unlike chabazite and Linde 4A, mordenite's maximum $\alpha_{CH_4\text{-}N_2}$ of 3.5 occurs within the boundaries of the map at about (300 K, 25 kPa). The values of $\alpha_{CO_2\text{-}CH_4}$ shown in Figure 5B have values approximately greater than 2 at all temperatures and generally increase with temperature, with the maximum for chabazite of 11.8 occurring at (370 K, 25 kPa). As the temperature increases so does the dependence of $\alpha_{CO_2\text{-}CH_4}$ on pressure, with Linde 4A exhibiting the most sensitivity. An inferred $\alpha_{CO_2\text{-}CH_4}$ of nearly 40 is predicted at (400 K, 25 kPa) for Linde 4A, which suggests that adsorption measurements of CH_4 + CO_2 mixtures could produce significant results around these conditions. Of course in such binary mixture adsorption experiments the partial pressure of the CH_4 would be much greater than 25 kPa if the experiment were to simulate a natural gas treatment process. It should also be noted that the adsorbent capacity decreases with increasing temperature; however, the gain in selectivity may compensate sufficiently for this in terms of the PSA bed sizes required to treat a given flow rate of natural gas.

To evaluate the potential of each adsorbent for a kinetic-based separation, adsorption capacity data were measured as a function of time at 100 kPa for each gas at each temperature. The time-dependent fractional uptakes $F_i(t)$ were calculated, and the mass transfer coefficients κ_i were derived using the linear driving force model as discussed in the Measurements and Analysis section. Estimates of the κ_i extracted from the time-dependent data at

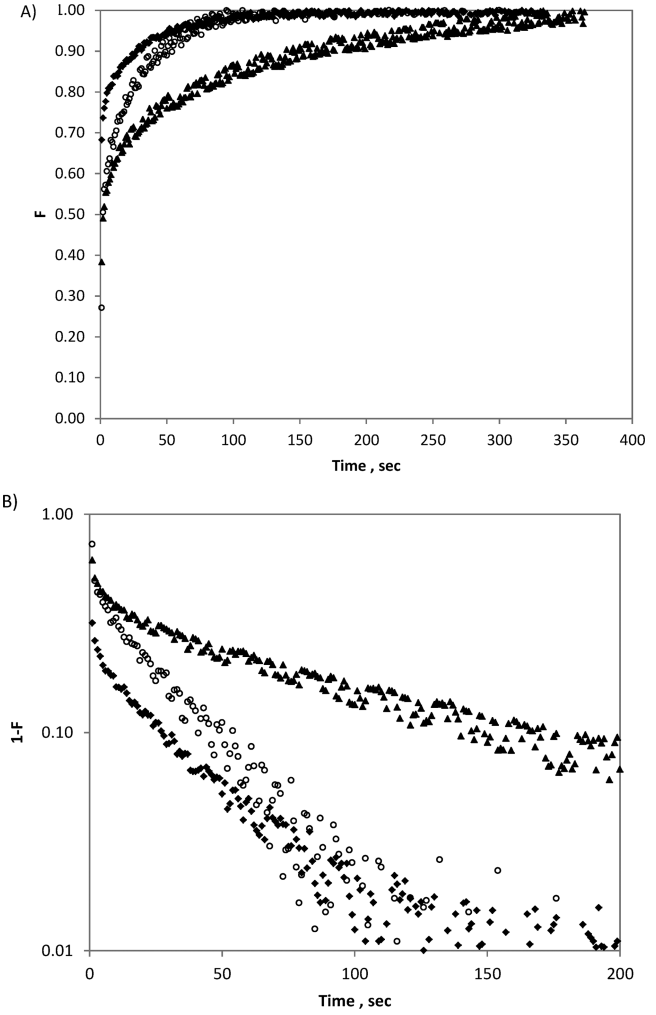

Figure 6. Fractional adsorption (eq 2) on chabazite at 302 K and 100 kPa as a function of time for CH_4, ◆; N_2, ○; and CO_2, ▲. (A) F as a function of time and (B) $(1 - F)$ vs t on a logarithmic scale, which can be used to produce more robust estimates of the respective mass transfer coefficients.

dx.doi.org/10.1021/je200817w |J. Chem. Eng. Data 2012, 57, 106–113

100 kPa are reported in Table 3. In Figure 6, example data are shown for each gas on chabazite at 302 K; Figure 6A shows $F_i(t)$ over the full 350 s required to reach equilibrium, while Figure 6B shows $1 - F_i(t)$ plotted on a log scale for the first 200 s at which point it is apparent that the noise in the N_2 and the CH_4 data is comparable to any remaining signal. For mordenite the $F_i(t)$ for N_2 and for CH_4 at 302 K were too noisy to extract any reliable values of κ_i. It is also apparent from Figure 6B that the uptake for all three gases appears to contain two different slopes, which could possibly correspond to two mass transfer coefficients; however the slope between (0 and 5) s is more likely the result of interference due to the rapid expansion of gas into the sample chamber as outlined by Jayaraman et al.,[34] while the second slope is likely to be characteristic of the adsorption uptake. For these reasons, the first few data points were excluded from our analysis. The determination of κ_i from the $F_i(t)$ is subject to quite significant uncertainties, the magnitude of which is difficult to estimate quantitatively. Yang[5] commented that the uncertainty of the diffusivity (which is proportional to κ_i) is about an order of magnitude. We estimate fractional repeatability of the κ_i obtained from our data to be 50 %. The κ_i determined in this work are of the same order of magnitude as those reported by other groups;[35−37] it should be noted, however, that measured values of the mass transfer coefficient depend quite sensitively on the size of the adsorbent particles, for example with pellets and single crystals having quite different values.

Of greater significance than the κ_i themselves are their ratios, which if sufficiently large could give rise to a kinetically based gas separation process. The inferred equilibrium and kinetic selectivities determined from the adsorption measurements at 100 kPa are listed in Table 3. The measured values of α_{ij} are all consistent with the values predicted using the Toth models, with Linde 4A at 302 K exhibiting the highest values of $\alpha_{CH_4\text{-}N_2}$ = 3.4 and $\alpha_{CO_2\text{-}CH_4}$ = 6.5. In most cases, the inferred β_{ij} are equal to or smaller than the corresponding α_{ij} because the ratios $(\kappa_{CH_4}/\kappa_{N_2}) \approx (\kappa_{CO_2}/\kappa_{CH_4}) \approx 1$, and thus in general we conclude that kinetic effects have a marginal or detrimental impact on the selectivities achievable with these zeolites. The notable exception is for Linde 4A at 273 K where κ_{CH_4} is between 2 and 3 times smaller than κ_{CO_2} and κ_{N_2}. In the latter case, this simply serves to again make the inferred $\beta_{CH_4\text{-}N_2} < \alpha_{CH_4\text{-}N_2}$. However, $(\kappa_{CO_2}/\kappa_{CH_4})$ = 2.8, and thus for Linde 4A the inferred kinetic selectivity for CO_2 over CH_4 at (273 K, 100 kPa) is 6.2. While this $\beta_{CO_2\text{-}CH_4}$ is comparable with the inferred $\alpha_{CO_2\text{-}CH_4}$ measured at (302 K, 100 kPa), it has the advantage of being at a lower temperature where the adsorbent's CO_2 capacity is 16 % larger than the capacity at 302 K. As noted by Ruthven,[27] it is relatively uncommon for the kinetic selectivity mechanism to act in the same direction as the equilibrium selectivity.

This result for Linde 4A encapsulates the essence of the screening approach described in this paper. The confluence of pure fluid capacities, mass transfer coefficients, and inferred selectivites for CH_4 and CO_2 on Linde 4A at low pressures in the temperature range (273 to 302) K, suggest that this may be a particularly fruitful region for subsequent adsorption measurements with CH_4 + CO_2 mixtures. Of course, this reflects the fact that the 4A molecular sieve is already used in a commercial process to treat natural gas with CO_2 mole fractions less than 0.02 down to the LNG specification;[22] however these results indicate it may be possible to improve upon such a process. For example, by operating a PSA bed of a given size at the lower temperature, it may be possible to remove more CO_2 because of the increase in adsorbent capacity. Therefore, the process could potentially treat a higher flow rate gas stream or one that is more contaminated. The viability and design of any improved PSA separation process will depend critically on the results of the additional measurements that must be made with mixtures and at higher pressures; such measurements have been made for the chabazite by Watson et al.[38] Nevertheless, in the pursuit of establishing an adsorbent's potential for a given gas separation application, efficient pure fluid screening measurements such as those described here are essential steps in targeting and designing the next phase of mixture measurements where the potential parameter space to be searched is significantly larger.

■ ASSOCIATED CONTENT

Supporting Information. Natural chabazite and Linde 4A data for nitrogen, methane, and carbon dioxide at (302, 272, and 248) K and H^+ modenite data for nitrogen, methane, and carbon dioxide at (302 and 272) K (SI Tables 1 to 9); XRD spectra of natural chabazite (SI Figure 1); and XRF analysis data of natural chabazite (SI Table 10). This material is available free of charge via the Internet at http://pubs.acs.org.

■ AUTHOR INFORMATION

Corresponding Author

*E-mail: eric.may@uwa.edu.au.

Funding Sources

This research was funded by Chevron Energy Technology Company, the Western Australian Energy Research Alliance, and the Australian Research Council (Project LP0776928).

■ ACKNOWLEDGMENT

We thank Zeox Corporation, TOSOH Corporation, and Sigma-Aldrich (Australia) for supplying the zeolites studied in this work and Dr. Nick Burke and Dr. Yunxia Yang of CSIRO Earth Sciences and Resource Engineering for assistance with the XRF analysis.

■ REFERENCES

(1) *International Energy Outlook*; Energy Information Administration, Office of Integrated Analysis and Forecasting, U.S. Deptartment of Energy: Washington, DC, 2009.

(2) Kidnay, A. J.; Parrish, W. *Fundamentals of Natural Gas Processing*; CRC Press: Boca Raton, FL, 2006.

(3) Section 2 Product Specifications. In *Engineering Data Book*, 12th ed.; Gas Processors Suppliers Association: Tulsa, OK, 2004; Vol. 2.

(4) *BP Statistical Review of World Energy*; BP: London, U.K., 2011.

(5) Yang, R. T. *Gas Separation by Adsorption Processes*; Butterworths: Boston, 1987; p 352.

(6) Cavenati, S.; Grande, C. A.; Rodrigues, A. E. Adsorption Equilibrium of Methane, Carbon Dioxide, and Nitrogen on Zeolite 13x at High Pressures. *J. Chem. Eng. Data* **2004**, *49*, 1095–1101.

(7) Mitariten, M. In *Nitrogen Removal from Natural Gas with the Molecular Gate™ Adsorption Process*, 88th Annual Convention of the Gas Processors Association 2009, San Antonio, Texas, March 8−11, 2009; Gas Processors Association: San Antonio, TX, 2009; pp 544−555.

(8) Toreja, J.; Chan, N.; VanNostrand, B.; Dickinson, J. P. Rotary-Valve, Fast-Cycle Pressure Swing Adsorption Technology Allows West Coast Platofrm to Meet Tight California Specifications and Recover Stranded Gas. In *Laurance Reid Gas Conditioning Conference*, University of Oklahoma: Norman, OK, 2011.

(9) Cavenati, S.; Grande, C. A.; Rodrigues, A. E. Separation of Methane and Nitrogen by Adsorption on Carbon Molecular Sieve. *Sep. Sci. Technol.* **2005**, *40*, 2721–2743.

(10) Cavenati, S.; Grande, C. A.; Rodrigues, A. E. Separation of $CH_4/CO_2/N_2$ Mixtures by Layered Pressure Swing Adsorption for Upgrade of Natural Gas. *Chem. Eng. Sci.* **2006**, *61*, 3893–3906.

(11) Jayaraman, A.; Chiao, A. S.; Padin, J.; Yang, R. T.; Munson, C. L. Kinetic Separation of Methane/Carbon Dioxide by Molecular Sieve Carbons. *Sep. Sci. Technol.* **2002**, *37*, 2505–2528.

(12) Watson, G.; May, E. F.; Graham, B. F.; Trebble, M. A.; Trengove, R. D.; Chan, K. I. Equilibrium Adsorption Measurements of Pure Nitrogen, Carbon Dioxide, and Methane on a Carbon Molecular Sieve at Cryogenic Temperatures and High Pressure. *J. Chem. Eng. Data* **2009**, *54*, 2701–2707.

(13) Ackley, M. W.; Giese, R. F.; Yang, R. T. Clinoptilolite - Untapped Potential for Kinetic Gas Separations. *Zeolites* **1992**, *12*, 780–788.

(14) Ackley, M. W.; Rege, S. U.; Saxena, H. In *Application of Natural Zeolites in the Purification and Separation of Gases*; Elsevier Science Bv: New York, 2003; pp 25−42.

(15) Delgado, J. A.; Uguina, M. A.; Gomez, J. M. Adsorption Equilibrium of Carbon Dioxide, Methane and Nitrogen onto Mordenite at High Pressures. In *Molecular Sieves: From Basic Research to Industrial Applications*, Parts A and B; Cejka, J., Zilkova, N., Nachtigall, P., Eds.; Elsevier Science Bv: Amsterdam, 2005; Vol. 158, pp 1065−1072.

(16) Jayaraman, A.; Hernandez-Maldonado, A. J.; Yang, R. T.; Chinn, D.; Munson, C. L.; Mohr, D. H. Clinoptilolites for Nitrogen/Methane Separation. *Chem. Eng. Sci.* **2004**, *59*, 2407–2417.

(17) Bae, Y.-S.; Farha, O. K.; Hupp, J. T.; Snurr, R. Q. Enhancement of CO_2/N_2 Selectivity in a Metal-Organic Framework by Cavity Modification. *J. Mater. Chem.* **2009**, *19*, 2131–2134.

(18) Saha, D.; Bao, Z.; Jia, F.; Deng, S. Adsorption of CO_2, CH_4, N_2O, and N_2 on Mof-5, Mof-177, and Zeolite 5a. *Environ. Sci. Technol.* **2010**, *44*, 1820–1826.

(19) Saha, D.; Deng, S. G. Adsorption Equilibria and Kinetics of Carbon Monoxide on Zeolite 5a, 13x, Mof-5, and Mof-177. *J. Chem. Eng. Data* **2009**, *54*, 2245–2250.

(20) Majumdar, B.; Bhadra, S. J.; Marathe, R. P.; Farooq, S. Adsorption and Diffusion of Methane and Nitrogen in Barium Exchanged Ets-4. *Ind. Eng. Chem. Res.* **2011**, *50*, 3021–3034.

(21) Marathe, R. P.; Farooq, S.; Srinivasan, M. P. Effects of Site Occupancy, Cation Relocation, and Pore Geometry on Adsorption Kinetics in Ets-4. *J. Phys. Chem. B* **2005**, *109*, 3257–3261.

(22) UOP *Contaminant Removal from Natural Gas Streams*. http://www.uop.com/products/adsorbents/natural-gas/#natural-gas-adsorbents (accessed July 19, 2011).

(23) Webb, P. A.; Orr, C. *Analytical Methods in Fine Particle Technology*; Micromeritics Instrument Corp: Norcross, GA, 1997.

(24) Toth, J. State of Equations of the Solid-Gas Interface Layers. *Acta Chim. Hung.* **1971**, *69*, 311–328.

(25) Sircar, S.; Hufton, J. R. Why Does the Linear Driving Force Model for Adsorption Kinetics Work? *Adsorption* **2000**, *6*, 137–147.

(26) Gu, Y.; Lodge, T. P. Synthesis and Gas Separation Performance of Triblock Copolymer Ion Gels with a Polymerized Ionic Liquid Mid-Block. *Macromolecules* **2011**, *44*, 1732–1736.

(27) Ruthven, D. M. Molecular Sieve Separations. *Chem. Ing. Tech.* **2011**, *83*, 44–52.

(28) Sing, K. S. W.; Everett, D. H.; Haul, R. A. W.; Moscou, L.; Pierotti, R. A.; Rouquerol, J.; Siemieniewska, T. Reporting Physisorption Data for Gas Solid Systems with Special Reference to the Determination of Surface-Area and Porosity (Recommendations 1984). *Pure Appl. Chem.* **1985**, *57*, 603–619.

(29) Breck, D. W. *Zeolite Molecular Sieves: Structure, Chemistry, and Use*; Wiley: New York, 1974.

(30) Ridha, F. N.; Yang, Y. X.; Webley, P. A. Adsorption Characteristics of a Fully Exchanged Potassium Chabazite Zeolite Prepared from Decomposition of Zeolite Y. *Microporous Mesoporous Mater.* **2009**, *117*, 497–507.

(31) Delgado, J. A.; Uguina, M. A.; Gomez, J. M.; Ortega, L. Adsorption Equilibrium of Carbon Dioxide, Methane and Nitrogen onto Na- and H-Mordenite at High Pressures. *Sep. Purif. Technol.* **2006**, *48*, 223–228.

(32) Habgood, H. W. Kinetics of Molecular-Sieve Action. Sorption of Nitrogen/Methane Mixtures by Linde Molecular Sieve 4a. *Can. J. Chem.* **1958**, *36*, 1384–1397.

(33) Breck, D. W. Crystalline Molecular Sieves. *J. Chem. Educ.* **1964**, *41*, 678.

(34) Jayaraman, A.; Yang, R. T. *Diffusion of Nitrogen and Methane in Clinoptilolites - Tailored for N_2/CH_4 Separation*; Micromeritics: Norcross, GA, 2009; http://www.micromeritics.com.

(35) Yucel, H.; Ruthven, D. M. Diffusion of CO_2 in 4a and 5a Zeolite Crystals. *J. Colloid Interface Sci.* **1980**, *74*, 186–195.

(36) Ruthven, D. M.; Lee, L.-K.; Yucel, H. Kinetics of Non-Isothermal Sorption in Molecular Sieve Crystals. *AIChE J.* **1980**, *26*, 16–23.

(37) Mohr, R. J.; Vorkapic, D.; Rao, M. B.; Sircar, S. Pure and Binary Gas Adsorption Equilibria and Kinetics of Methane and Nitrogen on 4a Zeolite by Isotope Exchange Technique. *Adsorpt.-J. Int. Adsorpt. Soc.* **1999**, *5*, 145–158.

(38) Watson, G.; Jensen, N. K.; Rufford, T. E.; Chan, K. I.; May, E. F. Volumetric Adsorption Measurements of N_2, CO_2, CH_4, and a CO_2 + CH_4 Mixture on a Natural Chabazite from 5 to 3000 kPa. *J. Chem. Eng. Data* **2011**, submitted.